American College of
Neuropsychopharmacology

ARTICLE

Check for updates

Reductions in rostral anterior cingulate GABA are associated with stress circuitry in females with major depression: a multimodal imaging investigation

Maria Ironside[1,2], Amelia D. Moser[1,3], Laura M. Holsen [ID][4,5,6], Chun S. Zuo[4,7], Fei Du [ID][4,7,8], Sarah Perlo[1], Christine E. Richards[1], Jessica M. Duda[1], Xi Chen[4,7,8], Lisa D. Nickerson[4,7], Kaylee E. Null[1], Nara Nascimento[1], David J. Crowley[1], Madhusmita Misra[4,9], Jill M. Goldstein [ID][4,10,11,12] and Diego A. Pizzagalli [ID][1,4,7,12][✉]

The interplay between cortical and limbic regions in stress circuitry calls for a neural systems approach to investigations of acute stress responses in major depressive disorder (MDD). Advances in multimodal imaging allow inferences between regional neurotransmitter function and activation in circuits linked to MDD, which could inform treatment development. The current study investigated the role of the inhibitory neurotransmitter GABA in stress circuitry in females with current and remitted MDD. Multimodal imaging data were analyzed from 49 young female adults across three groups (current MDD, remitted MDD (rMDD), and healthy controls). GABA was assessed at baseline using magnetic resonance spectroscopy, and functional MRI data were collected before, during, and after an acute stressor and analyzed using a network modeling approach. The MDD group showed an overall lower cortisol response than the rMDD group and lower rostral anterior cingulate cortex (ACC) GABA than healthy controls. Across groups, stress decreased activation in the frontoparietal network (FPN) but increased activation in the default mode network (DMN) and a network encompassing the ventromedial prefrontal cortex–striatum–anterior cingulate cortex (vmPFC–Str–ACC). Relative to controls, the MDD and rMDD groups were characterized by decreased FPN and salience network (SN) activation overall. Rostral ACC GABA was positively associated with connectivity between an overlapping limbic network (Temporal–Insula–Amygdala) and two other circuits (FPN and DMN). Collectively, these findings indicate that reduced GABA in females with MDD was associated with connectivity differences within and across key networks implicated in depression. GABAergic treatments for MDD might alleviate stress circuitry abnormalities in females.

INTRODUCTION

Stress is an important contributor to the onset, maintenance, and relapse of major depressive disorder (MDD), with estimates suggesting that up to 80% of first major depressive episodes (MDEs) are preceded by major life events [1]. Evaluating the neurobiological effects of stress is therefore critical for understanding the pathophysiology of MDD. Females are at twice the risk for developing MDD as males; thus identifying sex-dependent neural responses to negative stress in MDD is important [2, 3]. Acute stress recruits bottom-up and/or top-down regulatory brain pathways [4]. Specifically, the brainstem senses perturbations to homeostatic equilibrium and directly activates the hypothalamus–pituitary–adrenal (HPA) axis and autonomic nervous system through the hypothalamus, resulting in the secretion of corticotropin from the pituitary gland and subsequently cortisol from the adrenal glands. In healthy individuals, the limbic system

(e.g., amygdala, hippocampus) is initially deactivated in response to stress [5, 6], which is correlated with cortisol secretion and thought to index a defense response. The prefrontal cortex is a key component of this response, providing top-down control to enable limbic deactivation [7]. This adaptive pattern is disrupted in MDD, with exaggerated limbic responses to stressors and reduced top-down control from frontal regions [8–10]. These neural effects are linked to HPA axis reactivity being altered in MDD [10], with studies reporting acute hyper- [11] and more chronically hypo-secretion of cortisol in response to stress, particularly in females (for a review, see ref. [12]). Such interplay between the HPA axis, cortical and limbic regions in stress circuitry call for a network approach to investigations of acute stress. Independent component analysis (ICA) is a data-driven technique that identifies intrinsically coupled functional networks and allows subsequent multivariate approaches [13] and network modeling [14].

[1]Center for Depression, Anxiety and Stress Research, McLean Hospital, Belmont, MA, USA. [2]Laureate Institute for Brain Research, Tulsa, OK, USA. [3]University of Colorado Boulder, Boulder, CO, USA. [4]Harvard Medical School, Boston, MA, USA. [5]Divison of Women's Health, Department of Medicine, Brigham & Women's Hospital, Boston, MA, USA. [6]Department of Psychiatry, Brigham & Women's Hospital, Boston, MA, USA. [7]McLean Imaging Center, McLean Hospital, Belmont, MA, USA. [8]Schizophrenia and Bipolar Research Program, McLean Hospital, Belmont, MA, USA. [9]Division of Pediatric Endocrinology, Massachusetts General Hospital, Boston, MA, USA. [10]Department of Psychiatry, Massachusetts General Hospital, Boston, MA, USA. [11]Department of Obstetrics and Gynecology, Massachusetts General Hospital, Boston, MA, USA. [12]These authors contributed equally: Jill M. Goldstein, Diego A. Pizzagalli. [✉]email: dap@mclean.harvard.edu

However, the many networks uncovered by this data-driven approach raises potential multiple comparison issues.

To guide our thinking around the networks associated with stress and psychopathology we relied on Menon's triple network model [15], which identifies networks important for understanding cognitive dysfunction across psychiatric disorders [16, 17]. These include the frontoparietal control network (FPN), important for cognitive control and adaptive behavioral regulation, the default mode network (DMN), implicated in self-referential mentation, and the salience network (SN), critical in the detection and mapping of salient external and internal inputs. The FPN and SN typically increase during stimulus-driven cognitive and affective information processing, while the DMN de-activates during task engagement. In terms of responses to acute stress, connectivity between the FPN↔SN has been highlighted as crucial to shifting between vigilance and recovery [18]. In MDD, deficits have manifested as increased DMN activation [16, 17, 19], associated with increased rumination [20], and decreased ability to deactivate the DMN during cognitive or affective tasks. Reduced FPN activation is also observed in MDD [21, 22], suggesting diminished top-down control over limbic regions and aberrant SN mapping, which ultimately impacts switching between the FPN and DMN and is associated with symptom severity in MDD [23]. In line with this, evidence points to decreased connectivity between the FPN↔DMN and increased connectivity between the DMN↔SN [23, 24] in MDD. However, a recent meta-analysis [17] suggests increased connectivity between the FPN↔DMN. Therefore, further investigations are needed.

Studies of acute negative stress responses in healthy controls (HC) implicate regions such as the anterior cingulate cortex (ACC), basal ganglia, hippocampus, insula, amygdala, and frontal regions [6]. We previously demonstrated that these stress responses were significantly associated with steroid hormone responses in females [25]. A network modeling approach found increased SN amplitude [26] and decreased SN↔DMN connectivity after stress [19]. Moreover, among cortisol responders, increases in amygdala connectivity with the DMN, mPFC, OFC, and hippocampus emerged [27, 28]. In addition, under acute stress, decreases in amygdala connectivity with the dorsolateral prefrontal cortex (dlPFC) and ACC have also been reported in HC [29]. These findings suggest that stress increases connectivity within limbic regions and decreases connectivity between limbic and prefrontal regions, resulting in decreased top-down control. Critically, in individuals with current or remitted MDD (rMDD), acute stress delivered through the Montreal Imaging Stress Test (MIST) reduced activation in the vmPFC [30]; moreover, among those with rMDD, stress-related activation of the dlPFC and striatum, as well as hyperconnectivity between the striatum and amygdala, emerged [30, 31]. Collectively, these findings highlight interactions between limbic and cortical regions subserving the experience of, and reaction to, acute stress that are impaired in a partially trait-like fashion in MDD. Given this circuitry is highly sexually dimorphic and females have higher rates of MDD, an understanding of the neural responses within females will contribute importantly to the overall understanding of MDD [32].

Growing evidence indicates that network interactions are affected by neuromodulators, including γ-aminobutyric acid (GABA)—the main inhibitory neurotransmitter [33, 34]. Reduced GABA levels have been observed in cerebrospinal fluid [35] and cortical brain tissues [36] of patients with MDD. Magnetic resonance spectroscopy (MRS) quantifies in vivo GABA in brain regions of interest non-invasively, with findings indicating reduced prefrontal and ACC GABAergic transmission in acute stress [37] and in MDD [38, 39], which can be reversed with treatment [40–42]. Associations between GABA and large-scale network connectivity have been found in healthy samples [43, 44] and in post-partum depression [45]. However, relationships between GABA and large-scale network connectivity in the response to stress in depression are poorly understood.

In sum, the present study takes a multi-pronged approach combining multimodal neuroimaging (GABA MRS and functional magnetic resonance imaging (fMRI)) with network modeling to assess the effects of acute stress in females with MDD and, to examine putative trait characteristics in rMDD. We hypothesized that in this female sample MDD would be associated with a blunted cortisol response to stress (although this can be dependent on chronicity), reduced rACC and/or left dlPFC GABA levels, and MDD and rMDD would be associated with aberrant changes in network amplitude and between-network connectivity in the FPN, SN, and DMN. We also predicted that those with rMDD would show greater increases in top-down control signals in the FPN compared with MDD alone. Further, we hypothesized that lower rACC and dlPFC GABA would be associated with deficits in engaging and disengaging these networks under stress. Finally, we anticipated that GABA in regions overlapping with the networks of interest (rACC in SN and dlPFC in FPN) would moderate network amplitude/connectivity through increased inhibition in these regions.

MATERIALS, PATIENTS, AND METHODS
Participants
Fifty-one unmedicated females (aged 18–25) were recruited from the community (see Supplemental Table S1). They provided written informed consent to a protocol approved by the Partners Human Research Committee. Participants were assessed by a clinician (at two study sites with high inter-rater reliability, see Supplemental Information) using the Structured Clinical Interview for the DSM-5 (SCID-5; [46]). Nineteen participants were assessed as having current MDE (MDD group), 15 were fully remitted from at least one prior MDE (rMDD), and 17 were HC. Exclusion criteria included other comorbid psychiatric disorders (except for simple phobia, social anxiety, and generalized anxiety disorder if secondary to MDD), use of psychoactive drugs, recent recreational drug use, past substance use disorder, and more than five alcohol-related blackouts.

Procedure
The imaging session took place in the early follicular phase and in the afternoon (to control for diurnal variability of cortisol response) [47]. After IV insertion, participants entered the 3 T scanner and underwent a single ~45-min GABA MRS scan before completing an acute laboratory stressor task during fMRI. Based on extensive piloting before study onset, to improve the potency of the stressor following piloting, this protocol combined the MIST [48] and the Maastricht Acute Stress Test (MAST) [49] into a single hybrid stressor and compared measurements to baseline. As depicted in Fig. 1, participants carried out four blocks of arithmetic problems, each lasting ~3.5 min. Participants used a three-button touchpad to navigate left or right to the correct digit (0 through 9) on a rotary dial and submitted their answer with a top button press. During the first block (pre-MAST), no time pressure was imposed, and the participants received trial-by-trial feedback of their performance ("correct" and "incorrect"), constituting a "no-stress" baseline condition. After the first block, the scanner table was brought out and the participant (whilst still lying on the scanner table) was asked to complete a 12-min MAST protocol: two experimenters acting as "doctors" (whom the participant had not met yet) entered the scanner suite and gave instructions for the MAST task, which involved interleaving blocks of mental arithmetic (counting backward from a four-digit number out loud in steps of 17) and immersing their hand in ice-cold (0–2 °C) water. The length of the blocks was determined by a computer algorithm (thus, introducing unpredictability and uncontrollability) and the "doctors" provided an evaluation of the arithmetic task for a
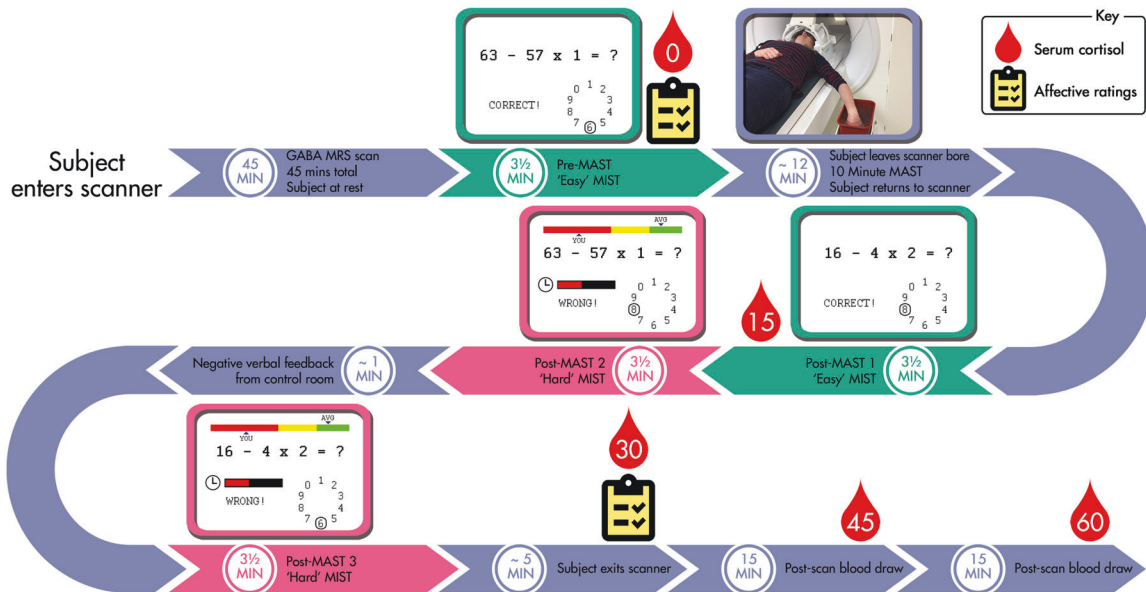
Fig. 1 **Combined stressor.** Initial BOLD acquisition under baseline condition (pre-MAST, untimed problems), followed by an acute stressor (MAST [49]), followed by subsequent BOLD acquisition under stress conditions (post-MAST1—untimed problems, post-MAST2—timed problems and progress bar), followed by negative verbal feedback over scanner intercom, followed by final BOLD acquisition (post-MAST3, timed problems with progress bar).

socio-evaluative component. After the MAST, the "doctors" informed the participant that they would continue monitoring their performance from the scanner suite. The table was returned to the scanner and the participant completed the second block of the MIST (post-MAST 1). In this block the problems were also untimed, providing a direct comparison to the pre-MAST block. In the third block of the MIST (post-MAST 2), stress was increased. Specifically, time pressure was imposed on each problem (calibrated by participants' no-stress responses), and performance monitoring compared to the purported average was shown on a mock performance bar. After the MAST 2 block, one "doctor" gave negative verbal feedback over the intercom, saying the performance was well below average and that the participant would need to improve in this final block to make the data useable. Finally, the participant completed another block (post-MAST 3), identical to post-MAST 2. Self-report affective ratings were collected pre- and post-stress.

MRI data acquisition and preprocessing
A 3 T Siemens MAGNETOM Prisma scanner (Siemens Medical Systems, Iselin, NJ) equipped with a 64-channel head coil was used to acquire high-resolution functional and structural MRI data (see Supplement). Functional MRI data were pre-processed using fMRIPrep 1.5.8 ([50]; RRID:SCR_016216), which is based on Nipype 1.4.1 ([51]; RRID:SCR_002502).

GABA MRS acquisition and processing
The T1-weighted structural images were used to place two independent voxels in the bilateral rACC (17.5 ml; $35 \times 20 \times 25$ mm^3) and left dlPFC (18.75 ml; $25 \times 30 \times 25$ mm^3) for MRS data collection (see Supplement and Supplemental Figs. S1 and S2) [52]. Single measurement GABA+ concentrations are reported as GABA+/water.

Blood cortisol collection and analysis
We previously published [11] method for acquiring HPA-axis hormone level changes in response to acute negative stress "in real-time" using serial blood samples was applied (see Supplement). Serum cortisol changes from stress were quantified using the area under the curve with respect to ground (AUCg) and with

respect to increasing (AUCi) calculations [53] to take into account all measurements and variability in the timing of cortisol peak following stress [54].

ICA of functional data
For a data-driven, circuit-level evaluation of stress-related neural changes, we ran a group ICA of the task fMRI data from all runs, and all participants temporally concatenated together using MELODIC in FSL. The model order (number of components estimated by ICA) was set between 10 and 40 for fine-tuning to estimate the model order that provided good separation between networks and between networks and noise. The resulting independent component maps were thresholded using Gaussian-gamma mixture modeling with a p value of ($p = 0.05$) to identify the signals in each component. Task activation networks were identified that correspond [55, 56] to resting-state networks highlighted in the triple network model. A dual regression approach [13] was used to extract network timecourses for each run for each participant that was then used to estimate the connectivity between each network pair and the amplitude (or task activation) of each network.

Model comparison approach
We tested for effects of stress and group using FSLNETS v0.6 [57] to implement general linear models with non-parametric permutation testing for estimation and inference (see Supplement). Our main outcome variables were partial correlations between network time-series (network pairs) and individual network amplitudes. GABA and cortisol AUC outliers (>1.5× outside the interquartile range) were first removed (cortisol: 2× HC, 1× MDD, dlPFC GABA: 1× MDD) and linear regression evaluated group differences using the lm function in R [58]. For repeated measures (main outcome network variables, self-report), mixed-effects regressions were conducted using the lmer4 package in R [58], a method that efficiently handles non-independence of repeated measures. We first specified an intercept-only null model to estimate the total systematic variance in the outcome variable where the outcome was regressed on a random effect variable for participants (random intercept). Next, we specified a three-step mixed-effects model with REML estimation. Firstly, we added the

main predictor—stress (4 levels/timepoints: pre-MAST, post-MAST1, post-MAST2, and post-MAST3) and secondly—group (3 levels: HC, MDD, and rMDD). Thirdly, we added the two-way interaction of stress and group. Model selection was identified using likelihood ratio tests [59]. We compared the null model (only random effects) with three models:

Null model: value ~ (1|participant)
Model 1 (main effect of stress): value ~ stress + (1|participant)
Model 2 (additive model): value ~ stress + group + (1|participant)
Model 3 (interactive model): value ~ stress + group + stress * group + (1|participant)

95% confidence intervals are reported. Power to achieve an R^2 of 0.3 using a random-effects model with two predictors (group and stress) was calculated using G*Power 3.1. For a one-tailed test, the required sample was 44 and for a two-tailed test, the required sample size was 50.

To leverage our multimodal data but also deal with possibly missing values more efficiently, mixed-effects regression in R was used to ascertain the effects of stress, group, GABA, cortisol AUC, and affective ratings on our main outcome variables of between-network covariance and network amplitude [58]. Specifically, we regressed connectivity and amplitude values on group, stress, rACC GABA, dlPFC GABA, cortisol, and affective ratings with a random effect for participants (intercept). Interactions between other predictors and stress were tested by comparing models with and without each interaction term. As the full sample did not have all of the measures (Supplemental Table S2), model selection was carried out using Akaike Information Criterion (AIC), a difference of ten between AICs being necessary for a model to be considered significantly improved [60].

RESULTS
Network maps
Visual inspection of the group ICA spatial maps in consultation with a neuroimaging biostatistician (L.N.) resulted in the selection of the model order 40 group ICA results for analyses. Based on Menon's triple network model [15] and additional regions of interest for stress tasks, a priori task networks of interest were as follows: (1) right FPN (Supplemental Fig. S3A); (2) ventromedial prefrontal, striatal, ACC network (vmPFC–Str–ACC; Fig. S3B); (3) SN (Fig. S3C); (4) a network including temporal regions, the insula, and amygdala (Temp–Ins–Amyg; Fig. S3D); and (5) the DMN (Fig. S3E). A maximum of five networks was selected to reduce multiple comparisons.

Stress results
A one-sample t test (against zero) on the AUCg and AUCi revealed that cortisol concentrations were significantly increased across all participants (AUCg: $t(33) = 15.96$, $p < 0.001$; AUCi: $t(34) = 2.60$, $p < 0.007$) indicating that the stressor elicited the intended effect. AUCg and AUCi were then regressed on a between-subjects factor of the group (HC, MDD, and rMDD). This model significantly predicted AUCg ($F(2, 31) = 3.73$, $p = 0.04$, $R^2 = 0.19$). Follow-up tests showed that MDD vs. rMDDs had lower AUCg ($t(31) = 2.71$, $p = 0.03$) (Supplemental Table S3 and Supplemental Fig. S4), but HC did not differ from the others (all $p > 0.3$). Similarly, for all affective rating measures, significant main effects of stress and MDD group emerged (Supplemental Fig. S5), indicating that the stressor increased negative affect and decreased positive affect across participants as expected [49] and that the MDD group had increased negative affect compared to the HC group.

GABA MRS results
GABA MRS values from the rACC and dlPFC were regressed on the group (HC, MDD, and rMDD). The model significantly predicted rACC GABA ($F(2, 40) = 3.23$, $p = 0.05$, $R^2 = 0.14$). Follow-up tests
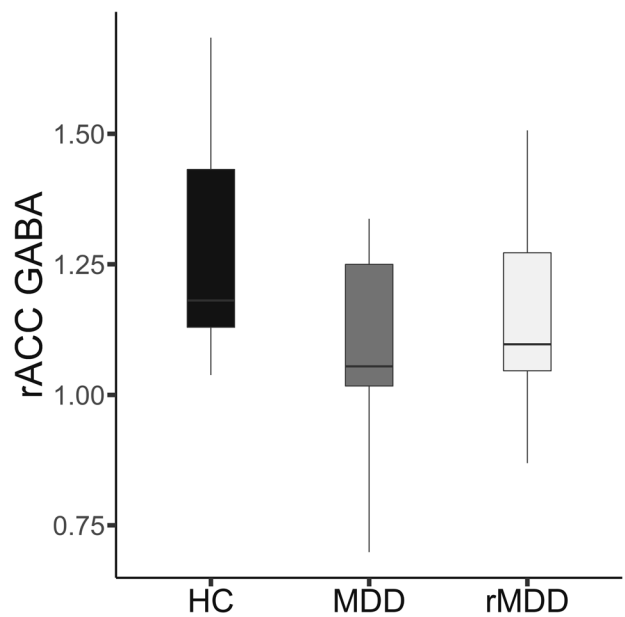

Fig. 2 Decreased rostral Anterior Cingulate cortex GABA in current major depressive disorder vs. healthy controls. The dark line inside the box represents the median. The top of the box is 75th percentile and the bottom of the box is the 25th percentile. The endpoints of the lines (aka whiskers) are at a distance of 1.5× interquartile range (the distance between 25th and 75th percentiles). HC ($N = 13$) mean (M) = 1.26, standard deviation (SD) = 0.20; MDD ($N = 17$) M = 1.10, SD = 0.16; rMDD ($N = 14$) M = 1.14, SD = 0.19.

showed that, as hypothesized, the MDD group had significantly lower levels of rACC GABA than HC ($t(40) = 2.49$, $p = 0.04$) (Fig. 2), whereas rMDDs did not ($t(40) = 1.74$, $p = 0.20$). A post hoc analysis showed that gray matter volume in the rACC did not differ between the HC and MDD groups ($t(40) = 0.22$, $p = 0.97$), although the rMDD group showed trends for lower gray matter volume in the rACC than the HCs ($t(40) = 2.31$, $p = 0.07$) and the MDDs ($t(40) = 2.23$, $p = 0.08$).

FMRI results: effects of stress and diagnosis
Network amplitude in the FPN was best explained by a model including stress + group (model 2 above), indicating a decrease in activation in this network from stress at post-MAST2 ($\beta = -0.13$, 95% CI: [−0.24 to −0.02]) and post-MAST3 ($\beta = -0.22$, 95% CI: [−0.33 to −0.11]), and an overall decrease in network amplitude in MDD ($\beta = -0.26$, 95% CI: [−0.12 to −0.040]) and rMDD ($\beta = -0.23$, 95% CI: [−0.37 to −0.08]) compared to HC (Fig. 3). Similarly, network amplitude in the SN was best explained by the stress + group model (model 2), indicating a decrease in activation for the MDD ($\beta = -0.28$, 95% CI: [−0.046 to −0.09]) and rMDD ($\beta = -0.19$, 95% CI: [−0.38 to −0.00]) groups compared to HC but the individual predictors were not significant.

Network amplitude in the vmPFC–Str–ACC network was best explained by a model including stress only (model 1), owing to increases in activation at post-MAST3 ($\beta = 0.44$, 95% CI: [0.23 to 0.65]). Network amplitude in the DMN was best explained by a model including stress only (model 1), with increases in activation at post-MAST1 ($\beta = 0.08$, 95% CI: [0.00 to 0.16]). There were no improvements on the null model for the Temp–Ins–Amyg network or any of the between-network connectivity pairs and the interactive model (model 3 above) did not fit any of the amplitude or connectivity data better than the stress + group model (model 2), suggesting either that neural response to stress did not vary systematically across groups or this study was underpowered to identify a significant interaction effect. The optimal base model parameters are shown in Table 1.
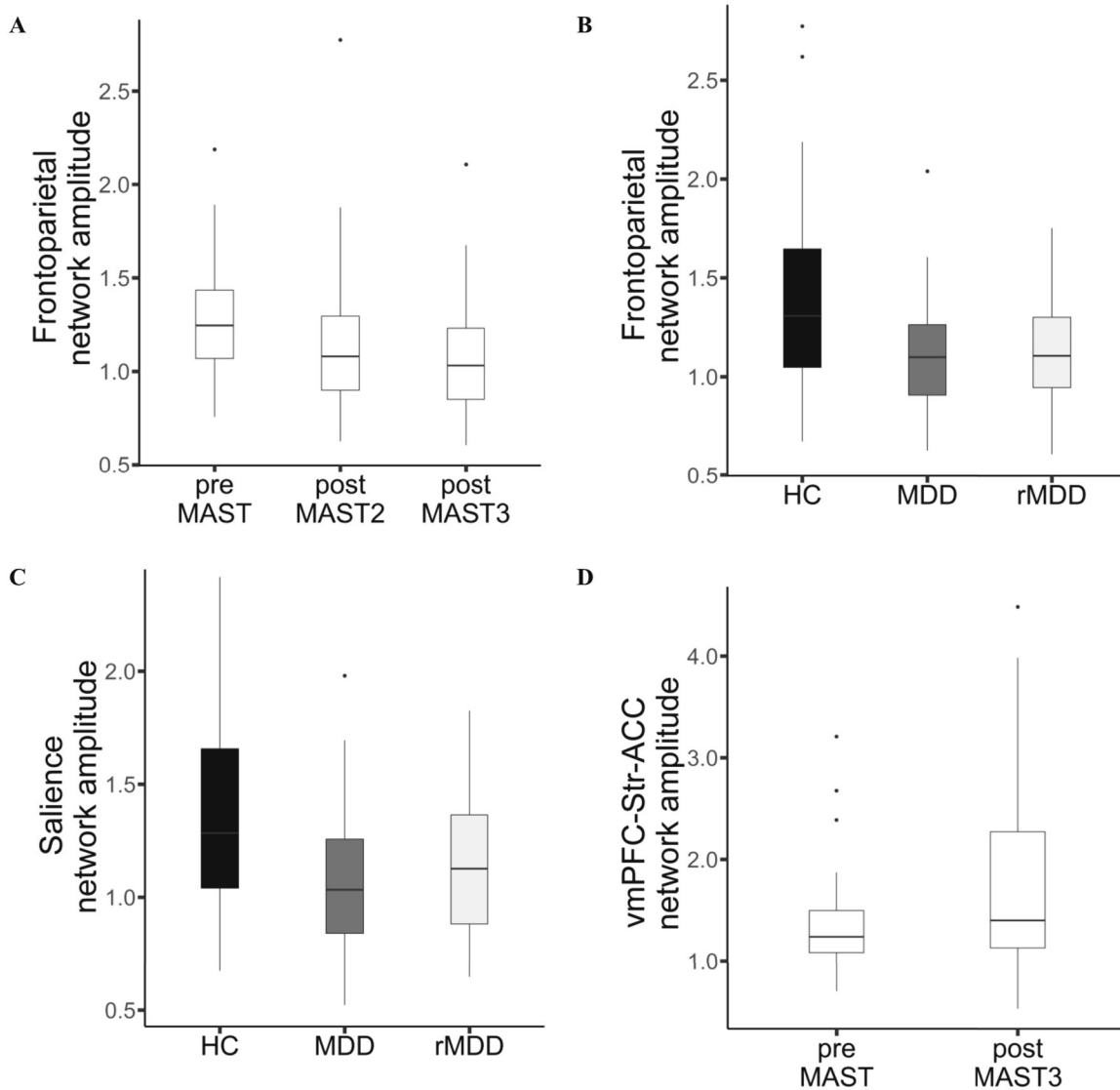
Fig. 3 Stress and diagnosis affect network amplitude. A Frontoparietal network amplitude decreased by stress. **B** Frontoparietal network amplitude decreased in MDD and rMDD. **C** Salience network amplitude decreased in MDD and rMDD. **D** vmPFC–Str–ACC network amplitude increased by stress. HC: $N = 17$; MDD: $N = 18$; rMDD: $N = 14$. The dark line inside the box represents the median. The top of the box is 75th percentile and the bottom of the box is the 25th percentile. The endpoints of the lines (i.e., whiskers) are at a distance of 1.5× interquartile range (the distance between 25th and 75th percentiles).

Table 1. Effects of group and stress on network amplitude response to stress in MDD and rMDD.

	FPN		vmPFC–Str–ACC		SN		DMN	
Predictors	β estimates	95% CI	β estimates	95% CI	β estimates	95% CI	β estimates	95% CI
(Intercept)	1.44	[1.32 to 1.56]	1.35	[1.17 to 1.53]	1.34	[1.19 to 1.48]	0.94	[0.87 to 1.01]
Time [post-Mast1]	0.04	[−0.07 to 0.15]	0.02	[−0.19 to 0.23]	0.04	[−0.05 to 0.14]	0.08	[0.00 to 0.16]
Time [post-Mast2]	−0.13	[−0.24 to −0.02]	0.21	[−0.00 to 0.42]	0.03	[−0.07 to 0.13]	−0.02	[−0.10 to 0.06]
Time [post-Mast3]	−0.22	[−0.33 to −0.11]	0.44	[0.23 to 0.65]	−0.02	[−0.12 to 0.08]	−0.07	[−0.15 to 0.01]
Group [MDD]	−0.26	[−0.40 to −0.12]			−0.28	[−0.46 to −0.09]		
Group [rMDD]	−0.23	[−0.37 to −0.08]			−0.19	[−0.38 to 0.00]		
Random effects								
σ^2	0.08		0.29		0.06		0.04	
τ_{00}	0.02 subject		0.14 subject		0.06 subject		0.03 subject	
ICC	0.23		0.33		0.5		0.4	
N	49 subject		49 subject		49 subject		49 subject	
Observations	194		194		194		194	
Marginal R^2/Conditional R^2	0.196/0.384		0.068/0.374		0.109/0.557		0.041/0.420	

FPN right frontoparietal network, *vmPFC-Str-ACC* ventromedial prefrontal cortex, ventral striatum and anterior cingulate cortex, *SN* salience network, *DMN* default mode network.

Association with affective ratings, cortisol, and GABA

To leverage the multimodal data, we compared extended mixed-effects models to examine the relationship between network amplitude/connectivity and the additional predictors rACC/dlPFC GABA, cortisol AUC, and affective ratings. Building on the initial group/stress analyses, the optimum base model (null model/model 1/model 2) was augmented with the additional predictors in a stepwise manner, and model AICs were compared. Models including AUC_G and AUC_I were directly compared using the same criteria. FPN network amplitude was best explained by a model that included rACC GABA, dlPFC GABA, and cortisol AUC_G ($R^2 = 0.32$), whereas a model including only rACC GABA best-explained vmPFC–Str–ACC activation ($R^2 = 0.36$). For SN, the model included rACC GABA, dlPFC GABA, Cortisol AUC_G, state anxiety change, and negative affect change ($R^2 = 0.36$). Extended models for the Temp–Ins–Amyg and DMN networks did not improve on the optimum base model (Supplemental Table S4).

Dimensional analyses of GABA and network connectivity/amplitude

Given the significant decrease in rACC GABA in the MDD group compared to HC, further analyses examined relationships between rACC GABA and network connectivity or amplitude. We adopted a dimensional approach, regressing connectivity/amplitude values on fixed effects of stress (pre-MAST, post-MAST1, post-MAST2, and post-MAST3), rACC GABA, and their interaction, with a per-participant random adjustment to the fixed intercept. Rostral ACC GABA was positively associated with between-network connectivity in two network pairs across all conditions; FPN↔Temp–Ins–Amyg ($\beta = 2.507$, 95% CI: [0.256 to 4.757]) and the Temp–Ins–Amyg↔DMN ($\beta = 2.226$, 95% CI: [0.141 to 4.311]). There were no interactions between rACC GABA and stress. Crucially, the rACC MRS voxel overlapped the Temp–Ins–Amyg network (Fig. 4).

DISCUSSION

Acute negative stress significantly increased cortisol across all females, although females with MDD had lower cortisol AUC_G than those with rMDD. In addition, females with MDD were characterized by decreased rACC GABA compared to healthy females. Three networks of interest were affected by acute stress across all groups. Specifically, the FPN network was characterized by decreased activation during the MIST task under acute stress, whereas the vmPFC–Str–ACC network and DMN networks showed increased stress-related activation. Irrespective of stress, females with MDD and rMDD were characterized by decreased FPN and SN activation compared to HCs. Critically, levels of GABA in the rACC were positively associated with activation in the SN and vmPFC-Str-ACC and negatively associated with activation in the FPN. Finally, dimensional analyses showed that rACC GABA was associated with increased connectivity between limbic regions (Temp–Ins–Amyg) and the FPN and DMN.

Together, these findings point to a key role for rACC GABA in downstream network activation and cortico-limbic between-network connectivity under negative stress. Rostral ACC GABA was reduced in MDD while females with MDD and rMDD showed decreased FPN and SN activation. This suggests that a deficit in rACC GABA may reflect impaired inhibition, which may be associated with deficient top-down control and aberrant salience mapping. Similar to prior findings in females with MDD [61], we observed a blunted cortisol response to stress in MDD. This finding may also be related to the number of depressive episodes or young age of the females, given that we previously reported differences in negative stress circuitry responses and hormonal physiology dependent on the age of females with MDD [2, 11]. Collectively, we speculate that these patterns highlight blunted stress response in MDD which may lead to decreased SN activation, thereby lowering demand on the FPN to exert top-down control. This was further supported by dimensional analyses showing that rACC GABA was associated with increases in connectivity between a limbic network (Temp–Ins–Amyg) and the FPN and DMN.

Healthy stress response circuitry involves salience mapping (SN) and top-down control over limbic regions (Temp–Ins–Amyg) by increasing connectivity with the FPN. Current findings suggest that the females with MDD and rMDD had reduced FPN and SN activation overall, highlighting impaired top-down control and compromised salience mapping. Findings showed increased stress-related amplitude across all groups in a network including vmPFC, striatum, and ACC. The vmPFC coordinates behavioral and physiological stress responses across multiple temporal and contextual domains [62] and is critical to active coping in acute stress response, which can become blunted with repeated life stress [63]. This is reinforced by prior findings in MDD and rMDD [30] showing reduced vmPFC activation to negative stress, although we did not see vmPFC group differences.
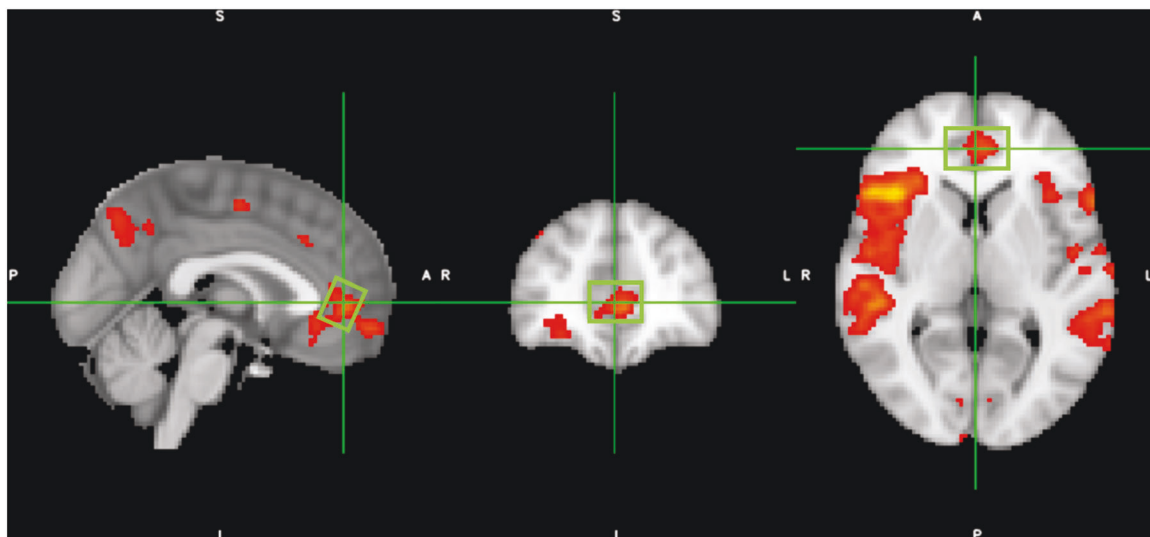
Fig. 4 Multimodal intersection of fMRI and MRS data. Overlap between Temp–Ins–Amyg network and approximate location of rostral anterior cingulate MRS voxel ($35 \times 20 \times 25$ mm^3).

GABA MRS data add a new dimension to the role of rACC inhibition in stress, with the addition of rACC GABA improving predictive models of amplitude in the FPN, SN, and vmPFC–Str–ACC. Taking a dimensional approach, higher rACC GABA was associated with higher connectivity between the Temp–Ins–Amyg network (which overlaps the MRS voxel) and two networks (FPN and DMN) implicated in MDD. The Temp–Ins–Amyg network contains regions from the cingulo-opercular network, which is characterized as a critical hub with pervasive other network connectivity [15]. Decreased GABAergic inhibition in the rACC in MDD could result in impaired communication between regions involved in the stress response which manifests as reduced connectivity of this network including limbic regions (Temp–Ins–Amyg) with the FPN and DMN. We suggest that stress-induced activation in the Temp–Ins–Amyg is critically affected by its connectivity with other regions, namely the FPN and the DMN, and that rACC GABA may reduce the influence of the limbic system on this critical stress hub. A recent trial of the positive allosteric modulator of $GABA_A$ receptors has shown promising results in the treatment of MDD [64]. The additional complexity of the model that should be noted is that the measure of total tissue GABA does not necessarily reflect inhibitory function. Finally, the lack of findings for dlPFC GABA could be explained through its indirect role in regulating the stress response via top-down cognitive control, rather than the more direct role of the rACC in inhibiting arousal.

Limitations of the study include potential stress from IV insertion, a lack of behavioral measures or group differences in between-network connectivity, participants taking contraception, modest sample size, and shorter duration blocks used for this task-based fMRI study than are typically used in resting-state designs. However, our repeated measures design, the inclusion of only females, and controlling of menstrual cycle and time of day likely improved our statistical power. All our reported effects were the main effects of stress, group, or rACC GABA. There were no interactions of stress X group, suggesting that the clinical groups did not respond to stress differently to the HCs. There are also potential networks that we did not examine, due to the need to reduce multiple comparisons. Even so, the SN model, group differences in rACC GABA and their association with network connectivity did not survive correction for a number of regions/networks examined. A stepwise model comparison approach was taken with the aim of parsimony and inclusion of all data points. However, this approach is less hypothesis-driven than more traditional approaches. Nevertheless, brain activation, connectivity, and physiology differences between groups provide insights into understanding differential strategies to maintain similar behavioral responses. Trauma was not examined in this study and could be a key factor in stress sensitivity. Moreover, the young age of the sample, lack of comorbidities, and limited ecological validity of acute laboratory stressors limit generalizability. Finally, future studies could leverage advances in functional MRS [65] to examine how changes in GABA unfold over the course of a stressor.

In sum, we found that stress increased amplitude in a network including the vmPFC, striatum, and ACC, and in the DMN, and reduced amplitude in the FPN. In addition, compared to HC, females with MDD and rMDD showed decreased network amplitude in the SN and FPN, implicating impaired trait-like top-down control and salience mapping. Importantly, rostral ACC GABA was associated with network amplitude in the SN, FPN, and vmPFC-Str-ACC, and connectivity between an overlapping limbic network (Temp–Ins–Amyg) and two circuits (FPN and DMN) critical to MDD pathophysiology. Together, these novel findings suggest that inhibitory GABAergic mechanisms have downstream effects on activation of, and connectivity between, circuits implicated in negative stress and pathophysiology in MDD.

REFERENCES

1. Hammen C. Stress and depression. Annu Rev Clin Psychol. 2005;1:293–319.
2. Holsen LM, Spaeth SB, Lee J-H, Ogden LA, Klibanski A, Whitfield-Gabrieli S, et al. Stress response circuitry hypoactivation related to hormonal dysfunction in women with major depression. J Affect Disord. 2011;131:379–87.
3. Goldstein JM, Jerram M, Abbs B, Whitfield-Gabrieli S, Makris N. Sex differences in stress response circuitry activation dependent on female hormonal cycle. J Neurosci. 2010;30:431–8.
4. Ulrich-Lai YM, Herman JP. Neural regulation of endocrine and autonomic stress responses. Nat Rev Neurosci. 2009;10:397–409.
5. Pruessner JC, Dedovic K, Khalili-Mahani N, Engert V, Pruessner M, Buss C, et al. Deactivation of the limbic system during acute psychosocial stress: evidence from positron emission tomography and functional magnetic resonance imaging studies. Biol Psychiatry. 2008;63:234–40.
6. Dedovic K, D'Aguiar C, Pruessner JC. What stress does to your brain: a review of neuroimaging studies. Can J Psychiatry. 2009;54:6–15.
7. Friedman MJ. The human stress response. A Practical Guide to PTSD Treatment: Pharmacological and Psychotherapeutic Approaches. Washington, DC, US: American Psychological Association; 2015. p. 9–19.
8. Siegle GJ, Thompson W, Carter CS, Steinhauer SR, Thase ME. Increased amygdala and decreased dorsolateral prefrontal BOLD responses in unipolar depression: related and independent features. Biol Psychiatry. 2007;61:198–209.
9. Muller J, Corodimas KP, Fridel Z, LeDoux JE. Functional inactivation of the lateral and basal nuclei of the amygdala by muscimol infusion prevents fear conditioning to an explicit conditioned stimulus and to contextual stimuli. Behav Neurosci. 1997;111:683–91.
10. Goldstein, JM, Holsen, L, Cherkerzian, S, Misra, M, Handa R. Neuroendocrine mechanisms of depression: clinical and preclinical evidence. In: Charney DS, Nestler EJ, Sklar P, editors. Charney & Nestler's Neurobiology of Mental Illness. Oxford: Oxford University Press; 2017. p. 365–75.
11. Holsen LM, Lancaster K, Klibanski A, Whitfield-Gabrieli S, Cherkerzian S, Buka S, et al. HPA-axis hormone modulation of stress response circuitry activity in women with remitted major depression. Neuroscience. 2013;250:733–42.
12. Zorn JV, Schür RR, Boks MP, Kahn RS, Joëls M, Vinkers CH. Cortisol stress reactivity across psychiatric disorders: a systematic review and meta-analysis. Psychoneuroendocrinology. 2017;77:25–36.
13. Nickerson LD, Smith SM, Öngür D, Beckmann CF. Using dual regression to investigate network shape and amplitude in functional connectivity analyses. Front Neurosci. 2017;11:115.
14. Smith SM, Miller KL, Salimi-Khorshidi G, Webster M, Beckmann CF, Nichols TE, et al. Network modelling methods for FMRI. Neuroimage 2011;54:875–91.
15. Menon V. Large-scale brain networks and psychopathology: a unifying triple network model. Trends Cogn Sci. 2011;15:483–506.
16. Mulders PC, van Eijndhoven PF, Schene AH, Beckmann CF, Tendolkar I. Resting-state functional connectivity in major depressive disorder: a review. Neurosci Biobehav Rev. 2015;56:330–44.
17. Kaiser RH, Andrews-Hanna JR, Wager TD, Pizzagalli DA. Large-scale network dysfunction in major depressive disorder: a meta-analysis of resting-state functional connectivity. JAMA Psychiatry 2015;72:603–11.
18. Hermans EJ, Henckens MJAG, Joëls M, Fernández G. Dynamic adaptation of large-scale brain networks in response to acute stressors. Trends Neurosci. 2014;37:304–14.
19. Vaisvaser S, Lin T, Admon R, Podlipsky I, Greenman Y, Stern N, et al. Neural traces of stress: cortisol related sustained enhancement of amygdala-hippocampal functional connectivity. Front Hum Neurosci. 2013;7:313.
20. Cooney RE, Joormann J, Eugène F, Dennis EL, Gotlib IH. Neural correlates of rumination in depression. Cogn Affect Behav Neurosci. 2010;10:470–78.
21. Liston C, Chen AC, Zebley BD, Drysdale AT, Gordon R, Leuchter B, et al. Default mode network mechanisms of transcranial magnetic stimulation in depression. Biol Psychiatry. 2014;76:517–26.
22. Lui S, Wu Q, Qiu L, Yang X, Kuang W, Chan RCK, et al. Resting-state functional connectivity in treatment-resistant depression. Am J Psychiatry. 2011;168:642–48.
23. Manoliu A, Meng C, Brandl F, Doll A, Tahmasian M, Scherr M, et al. Insular dysfunction within the salience network is associated with severity of symptoms and aberrant inter-network connectivity in major depressive disorder. Front Hum Neurosci. 2014;7:930.
24. Abbott CC, Lemke NT, Gopal S, Thoma RJ, Bustillo J, Calhoun VD, et al. Electroconvulsive therapy response in major depressive disorder: a pilot functional network connectivity resting state FMRI investigation. Front Psychiatry. 2013;4:10.
25. Goldstein JM, Jerram M, Poldrack R, Ahern T, Kennedy DN, Seidman LJ, et al. Hormonal cycle modulates arousal circuitry in women using functional magnetic resonance imaging. J Neurosci. 2005;25:9309–16.
26. van Marle HJF, Hermans EJ, Qin S, Fernandez G. Enhanced resting-state connectivity of amygdala in the immediate aftermath of acute psychological stress. Neuroimage. 2010;53:348–54.

27. Dimitrov A, Demin K, Fehlner P, Walter H, Erk S, Veer IM. Differences in neural recovery from acute stress between cortisol responders and non-responders. Front Psychiatry. 2018;9:631.

28. Mareckova K, Holsen L, Admon R, Whitfield-Gabrieli S, Seidman LJ, Buka SL, et al. Neural-hormonal responses to negative affective stimuli: impact of dysphoric mood and sex. J Affect Disord. 2017;222:88–97.

29. Quaedflieg CWEM, van de Ven V, Meyer T, Siep N, Merckelbach H, Smeets T. Temporal dynamics of stress-induced alternations of intrinsic amygdala connectivity and neuroendocrine levels. PLoS ONE. 2015;10:e0124141.

30. Ming Q, Zhong X, Zhang X, Pu W, Dong D, Jiang Y, et al. State-independent and dependent neural responses to psychosocial stress in current and remitted depression. Am J Psychiatry. 2017;174:971–9.

31. Admon R, Holsen LM, Aizley H, Remington A, Whitfield-Gabrieli S, Goldstein JM, et al. Striatal hypersensitivity during stress in remitted individuals with recurrent depression. Biol Psychiatry. 2015;78:67–76.

32. Goldstein JM, Holsen L, Handa R, Tobet S. Fetal hormonal programming of sex differences in depression: linking women's mental health with sex differences in the brain across the lifespan. Front Neurosci. 2014;8:247.

33. Chen X, Fan X, Hu Y, Zuo C, Whitfield-Gabrieli S, Holt D, et al. Regional GABA concentrations modulate inter-network resting-state functional connectivity. Cereb Cortex. 2019;29:1607–18.

34. Northoff G, Walter M, Schulte RF, Beck J, Dydak U, Henning A, et al. GABA concentrations in the human anterior cingulate cortex predict negative BOLD responses in fMRI. Nat Neurosci. 2007;10:1515–7.

35. Gerner RH, Hare TA. CSF GABA in normal subjects and patients with depression, schizophrenia, mania, and anorexia nervosa. Am J Psychiatry. 1981;138:1098–101.

36. Gabbay V, Mao X, Klein RG, Ely BA, Babb JS, Panzer AM, et al. Anterior cingulate cortexγ-aminobutyric acid in depressed adolescents: Relationship to anhedonia. Arch Gen Psychiatry. 2012;69:139–49.

37. Hasler G, van der Veen JW, Grillon C, Drevets WC, Shen J. Effect of acute psychological stress on prefrontal GABA concentration determined by proton magnetic resonance spectroscopy. Am J Psychiatry. 2010;167:1226–31.

38. Sanacora G, Mason GF, Krystal JH. Impairment of GABAergic transmission in depression: new insights from neuroimaging studies. Crit Rev Neurobiol. 2000;14:23–45.

39. Hasler G, van der Veen JW, Tumonis T, Meyers N, Shen J, Drevets WC. Reduced prefrontal glutamate/glutamine and γ-aminobutyric acid levels in major depression determined using proton magnetic resonance spectroscopy. Arch Gen Psychiatry. 2007;64:193–200.

40. Hasler G, Neumeister A, Van Der Veen JW, Tumonis T, Bain EE, Shen J, et al. Normal prefrontal gamma-aminobutyric acid levels in remitted depressed subjects determined by proton magnetic resonance spectroscopy. Biol Psychiatry. 2005;58:969–73.

41. Sanacora G, Mason GF, Rothman DL, Krystal JH. Increased occipital cortex GABA concentrations in depressed patients after therapy with selective serotonin reuptake inhibitors. Am J Psychiatry. 2002;159:663–5.

42. Sanacora G, Mason GF, Rothman DL, Hyder F, Ciarcia JJ, Ostroff RB, et al. Increased cortical GABA concentrations in depressed patients receiving ECT. Am J Psychiatry. 2003;160:577–9.

43. Levar N, Van Doesum TJ, Denys D, Van Wingen GA. Anterior cingulate GABA and glutamate concentrations are associated with resting-state network connectivity. Sci Rep. 2019;9:1–8.

44. Kapogiannis D, Reiter DA, Willette AA, Mattson MP. Posteromedial cortex glutamate and GABA predict intrinsic functional connectivity of the default mode network. Neuroimage. 2013;64:112–119.

45. Deligiannidis KM, Fales CL, Kroll-Desrosiers AR, Shaffer SA, Villamarin V, Tan Y, et al. Resting-state functional connectivity, cortical GABA, and neuroactive steroids in peripartum and peripartum depressed women: a functional magnetic resonance imaging and spectroscopy study. Neuropsychopharmacology. 2019;44:546–54.

46. First MB. Structured clinical interview for the DSM (SCID). Encycl Clin Psychol. 2014;1–6.

47. Miller R, Stalder T, Jarczok M, Almeida DM, Badrick E, Bartels M, et al. The CIRCORT database: Reference ranges and seasonal changes in diurnal salivary cortisol derived from a meta-dataset comprised of 15 field studies. Psychoneuroendocrinology. 2016;73:16–23.

48. Dedovic K, Renwick R, Mahani NK, Engert V, Lupien SJ, Pruessner JC. The Montreal Imaging Stress Task: using functional imaging to investigate the effects of perceiving and processing psychosocial stress in the human brain. J Psychiatry Neurosci. 2005;30:319–25.

49. Smeets T, Cornelisse S, Quaedflieg CWEM, Meyer T, Jelicic M, Merckelbach H. Introducing the Maastricht Acute Stress Test (MAST): a quick and non-invasive approach to elicit robust autonomic and glucocorticoid stress responses. Psychoneuroendocrinology. 2012;37:1998–2008.

50. Esteban O, Markiewicz CJ, Blair RW, Moodie CA, Isik AI, Erramuzpe A, et al. fMRIPrep: a robust preprocessing pipeline for functional MRI. Nat Methods. 2019;16:111–6.

51. Gorgolewski K, Burns CD, Madison C, Clark D, Halchenko YO, Waskom ML, et al. Nipype: a flexible, lightweight and extensible neuroimaging data processing framework in python. Front Neuroinform. 2011;5:13.

52. Duda JM, Moser AD, Zuo CS, Du F, Chen X, Perlo S, et al. Repeatability and reliability of GABA measurements with magnetic resonance spectroscopy in healthy young adults. Magn Reson Med. 2021;85:2359–69.

53. Pruessner JC, Kirschbaum C, Meinlschmid G, Hellhammer DH. Two formulas for computation of the area under the curve represent measures of total hormone concentration versus time-dependent change. Psychoneuroendocrinology. 2003;28:916–31.

54. Burke HM, Davis MC, Otte C, Mohr DC. Depression and cortisol responses to psychological stress: a meta-analysis. Psychoneuroendocrinology. 2005;30:846–56.

55. Smith SM, Fox PT, Miller KL, Glahn DC, Fox PM, Mackay CE, et al. Correspondence of the brain's functional architecture during activation and rest. Proc Natl Acad Sci USA. 2009;106:13040–45.

56. Nickerson LD. Replication of resting state-task network correspondence and novel findings on brain network activation during task fmri in the human connectome project study. Sci Rep. 2018;8:1–12.

57. Smith SM, Vidaurre D, Beckmann CF, Glasser MF, Jenkinson M, Miller KL, et al. Functional connectomics from resting-state fMRI. Trends Cogn Sci. 2013;17:666–82.

58. R Development Core Team. R: A Language and Environment for Statistical Computing; 2013.

59. Zuur A, Ieno EN, Walker N, Saveliev AA, Smith GM. Mixed effects models and extensions in ecology with R. Springer Science & Business Media; 2009.

60. Aho K, Derryberry D, Peterson T. Model selection for ecologists: the worldviews of AIC and BIC. Ecology 2014;95:631–6.

61. Burke HM, Fernald LC, Gertler PJ, Adler NE. Depressive symptoms are associated with blunted cortisol stress responses in very low-income women. Psychosom Med. 2005;67:211–6.

62. McKlveen JM, Myers B, Herman JP. The medial prefrontal cortex: coordinator of autonomic, neuroendocrine and behavioural responses to stress. J Neuroendocrinol. 2015;27:446–56.

63. Valenti O, Gill KM, Grace AA. Different stressors produce excitation or inhibition of mesolimbic dopamine neuron activity: response alteration by stress pre-exposure. Eur J Neurosci. 2012;35:1312–21.

64. Gunduz-Bruce H, Silber C, Kaul I, Rothschild AJ, Riesenberg R, Sankoh AJ, et al. Trial of SAGE-217 in patients with major depressive disorder. N Engl J Med. 2019;381:903–11.

65. White TL, Gonsalves MA. Imaging fast-acting drug effects in humans using 1H-MRS. ACS Chem Neurosci. 2020;11:2485–8.

AUTHOR CONTRIBUTIONS

Maria Ironside—Design of the work. Acquisition, analysis, and interpretation of data. Drafting of paper. Amelia D. Moser—Acquisition and analysis of data. Revision of the paper. Laura M. Holsen—Interpretation of data. Revision of the paper. Chun S. Zuo—Acquisition and analysis of data. Revision of the paper. Fei Du—Acquisition and analysis of data. Revision of the paper. Sarah Perlo —Acquisition and analysis of data. Christine E. Richards—Acquisition and analysis of data. Jessica M. Duda—Acquisition and analysis of data. Xi Chen—Analysis of data. Revision of the paper. Lisa D. Nickerson—Interpretation of data. Kaylee E. Null—Acquisition and analysis of data. Nara Nascimento—Acquisition and analysis of data. David J. Crowley—Acquisition

COMPETING INTERESTS
The authors declare no competing interests.

ADDITIONAL INFORMATION
Supplementary information The online version contains supplementary material
available at https://doi.org/10.1038/s41386-021-01127-x.

Correspondence and requests for materials should be addressed to D.A.P.

Reprints and permission information is available at http://www.nature.com/
reprints

Publisher's note Springer Nature remains neutral with regard to jurisdictional claims
in published maps and institutional affiliations.

SUPPLEMENTAL INFORMATION

Supplemental Methods

Participants

Screening took place at two study sites: McLean Hospital (Belmont, MA) and Brigham and Women's Hospital (Boston, MA). Inter-rater reliability was assessed using audiotapes of subject interviews that were independently, blindly rated by a second interviewer. Two McLean-based study interviewers rated audiotapes consisting of the SCID-5, Hamilton Depression Rating Scale (HDRS), and Quick Inventory of Depressive Symptomatology (QIDS) interviews conducted by one of the other three study interviewers, including one based at the BWH site. The 28 tapes (15% of the sample) that were included were randomly selected from within each of three diagnostic categories (MDD, remitted MDD, and not meeting criteria for either current or past depression) by a staff member not involved in the inter-rater reliability process. An intraclass correlation of 0.95 was obtained for the 17-item total HDRS score, and an intraclass correlation coefficient of 0.96 was obtained for the 16-item total QIDS score. Assessment of the diagnostic agreement of MDD vs. rMDD vs. no history of MDD yielded a kappa coefficient of 0.94. One MDD participant was excluded from analyses because of inconsistent reporting of clinical symptoms. Age of onset of first MDE did not differ significantly between the MDD (M = 16, SD = 3.25) and rMDD (M = 17.9, SD = 1.46) groups (t(30) = -1.98, p = 0.06). Recent recreational drug use was ruled out with a urine drug test carried out at screening and testing days. Exclusion for more than five alcohol-related blackouts follows findings on reductions in anterior cingulate GABA in those with a history of binge drinking (1). Participants were compensated for their time.

Procedure

The imaging session took place at a single site (McLean Hospital). This was timed to be in the early follicular phase (first seven days, although there were three participants, one in each group, who we allowed up to day 11 because of longer cycles) of the participants' menstrual cycle to control for hormonal variability and in the afternoon, to control for diurnal variability of cortisol response (2). Participants were unmedicated (if applicable, a washout period of six weeks for fluoxetine, two weeks for any other antidepressants or benzodiazepines, was required). Demographics are summarized in Supplemental Table S1. Participants were debriefed at the end of the study session. See Supplemental Table S2 for a summary of the final sample available for each measure.

Affective Ratings

To assess the effect of the stressor on self-report affect and state anxiety, participants completed affective ratings immediately before stress onset and 30 minutes after stress onset. Changes in positive and negative affect were measured using the Positive and Negative Affective Schedule (PANAS; (3)) and visual analog measurement scales (happy-sad, tense-anxious, friendly-hostile). Changes in state anxiety were measured using the State-Trait Anxiety Inventory, state subscale (STAI-S; (4)).

MRI data acquisition and preprocessing

Structural data were acquired with a T1-weighted magnetization-prepared rapid acquisition having gradient multi-echo (MPRAGE) imaging sequences with the following acquisition parameters: repetition time (TR) = 2530 ms; echo times (TE) = 1.69, 3.55, 5.41 and 7.27 ms; field of view = 256 mm; voxel dimensions = 1.0 x 1.0 x 1.0 mm^3; 176 slices. Functional MRI data were acquired using a gradient echo T2*-weighted echo planar imaging sequence with the following acquisition parameters: repetition time (TR) = 2000 ms; echo time (TE) = 30 ms; field of view = 204 mm; voxel dimension = 1.5 x 1.5 x 1.5 mm; 84 interleaved slices with a multiband acceleration factor of 3.

Anatomical data preprocessing

The T1-weighted (T1w) images were corrected for intensity non-uniformity (INU) with N4BiasFieldCorrection (5), distributed with ANTs 3.0.0 ((6), RRID:SCR_004757), and used as T1w-reference throughout the workflow. The T1w-reference was then skull-stripped with a Nipype implementation of the antsBrainExtraction.sh workflow (from ANTs), using OASIS30ANTs as target template. Brain tissue segmentation of cerebrospinal fluid (CSF), white-matter (WM) and gray-matter (GM) was performed on the brain-extracted T1w using fast (FSL 6.0.0, RRID:SCR_002823, (7)). Brain surfaces were reconstructed using recon-all (FreeSurfer 6.0.1, RRID:SCR_001847, (8)), and the brain mask estimated previously was refined with a custom variation of the method to reconcile ANTs-derived and FreeSurfer-derived segmentations of the cortical gray-matter of Mindboggle (RRID:SCR_002438, (9)). Volume-based spatial normalization to standard space (MNI152NLin6Asym) was performed through nonlinear registration with antsRegistration (ANTs 3.0.0), using brain-extracted versions of both T1w reference and the T1w template.

Functional data preprocessing

For each of the four BOLD runs, the following preprocessing was performed. First, a reference volume and its skull-stripped version were generated using a custom methodology of fMRIPrep. A deformation field to correct for susceptibility distortions was estimated based on fMRIPrep's fieldmap-less approach. The deformation field resulted from co-registering the BOLD reference to the same-participant T1w-reference with its intensity inverted (10, 11). Registration was performed with antsRegistration (ANTs 3.0.0), and the process regularized by constraining deformation to be nonzero only along the phase-encoding direction and modulated with an average fieldmap template (12). Based on the estimated susceptibility distortion, a corrected EPI (echo-planar imaging) reference was calculated for a more accurate co-registration with the anatomical reference. The BOLD reference was then co-registered to the T1w reference using bbregister (FreeSurfer), which implements boundary-based registration (13). Co-registration was configured with six degrees of freedom. Head-motion parameters with respect to the BOLD reference (transformation matrices, and six corresponding rotation and translation parameters) are estimated before any spatiotemporal filtering using mcflirt (FSL 6.0.0, (14)). BOLD runs were slice-time corrected using 3dTshift from AFNI 20190007 ((15), RRID:SCR_005927). The BOLD time-series were resampled to surfaces on the following spaces: fsaverage, MNI152NLin6Asym. The BOLD time-series (including slice-timing correction) were resampled onto their original, native space by applying a single, composite transform to correct for head-motion and susceptibility distortions. These resampled BOLD time-series will be referred to as preprocessed BOLD in original space, or just preprocessed BOLD. All resamplings can be performed with a single interpolation step by composing all the pertinent transformations (i.e., head-motion transform matrices, susceptibility distortion correction when available, and co-registrations to anatomical and output spaces). Gridded (volumetric) resampling was performed using antsApplyTransforms (ANTs), configured with Lanczos interpolation to minimize the smoothing effects of other kernels (16). Non-gridded (surface) resampling was performed using mri_vol2surf (FreeSurfer). Several confounding time-series were calculated based on the preprocessed BOLD: framewise displacement (FD), DVARS and three region-wise global signals. FD and DVARS were calculated for each functional run, both using their implementations in Nipype. Frames that exceeded a threshold of 0.5 mm FD or 1.5 standardised DVARS were annotated as motion outliers. Any participant with >20% motion outliers per run was excluded from analysis (1 rMDD excluded all runs, 1 HC excluded 1 run, 1 MDD excluded 1 run). Motion artifacts were estimated using independent component analysis (ICA-AROMA, (17)), visually checked and removed from the preprocessed BOLD on MNI space time-series using FSL's regfilt, after removal of non-steady state volumes and spatial smoothing with an isotropic, Gaussian kernel of 6mm FWHM (full-width half-maximum). The BOLD time-series were resampled into standard MNI space using antsApplyTransforms

(ANTs 3.0.0). Finally, the preprocessed, normalized BOLD runs were temporally filtered using a high bandpass of 150 sec and masked using the standard MNI152NLin6Asym T1 brain mask.

GABA MRS acquisition and processing

The T1-weighted structural images were used to place a voxel in the rACC (17.50 ml; 35 x 20 x 25 mm^3, Fig. S1) and left dlPFC (18.75 ml; 25 x 30 x 25 mm^3, Fig. S1) for MRS data collection. Proton GABA+ (macromolecular-contaminated) measurement employed a MEshcher-GArwood Point RESolved Spectroscopy (MEGA-PRESS) sequence obtained from the University of Minnesota with the acquisition frequency sitting at 3.0ppm and frequency-selective editing pulses, each with a duration of 17ms alternatively at 1.9 ppm (on) and 7.5 ppm (off) interleaved with the averages (18–21). MEGA-PRESS is an established MRS acquisition protocol for GABA detection that has demonstrated superior GABA test-retest reliability compared with other sequences, as described in detail in (22). The magnetic field homogeneity within the prescribed voxel was adjusted using a vendor-provided 3D shimming routine with additional water suppression optimization (completed by the same MRS physicist for all participants (Dr. Chun Zuo)).

GABA+ concentrations are reported as GABA+/water (a ratio of GABA+ to water multiplied by a scaling factor, reported in mM), and were small-volume corrected for percentage of tissue types in the voxels. LCModel fitting of the MRS data was assessed for quality based on Cramer-Rao Lower Bound (CRLB) values of <15% and signal-to-noise ratios of >20; additionally, spectra were visually assessed prior to analyses by MR physicists (Drs. Xi Chen and Fei Du) for severe baseline distortion, excluding one participant (final N = 43). GABA MRS data were not acquired for 5 participants (4 HC, 1 rMDD).

Blood cortisol collection and analysis

Trained technicians or nurses inserted a saline-lock IV line in the forearm. Blood acquisition commenced 60-80 minutes before participants entered the MRI scanner, with an in-scanner blood draw (baseline) one hour after entering the scanner, after the MRS scan and just prior to the start of the stressor (MAST0). Therefore the in-scanner baseline was acquired between 2-2.5 hours after IV insertion. All other blood draws were timed to the beginning of the MAST stressor. A 15-min in-scanner blood sample was drawn after the completion of the stressor (MAST15), followed by a 30-min in-scanner blood draw (MAST30) and 60-min (MAST60) and 90-min (MAST90) blood draws, out-of-scanner in a quiet room. Three additional blood draws occurred outside the scanner for a separate task to be published elsewhere. Subjects remained inside the bore of the magnet during in-scanner blood draws. The timing of these blood draws was based on the expected peak response (following the onset of the stressor) of cortisol between

10 and 60 min after stress onset. Hormone data were missing or not reported for some subjects due to poor IV access preventing blood acquisition during scanning (5 HC; 4 MDD, 4 rMDD). For those with partial data (3 HC, 1 MDD, 1 rMDD), when MAST0 and at least one other timepoint were available, missing timepoints were imputed using mixed-models regression. Approximately 5-20 mL of blood was sampled at each time point, allowed to clot for 30 min, spun in a refrigerated centrifuge, aliquoted, and stored frozen at -80°C. Cortisol was analyzed in duplicate with a commercial immunoassay kit (0.04 ug/dL; 4.4–6.7%): Immunoradiometric Assay (IRMA), DiaSorin, Inc., Stillwater, MN. Blood cortisol changes from stress were quantified using area under the curve (AUC) calculations (23). Area under the curve with respect to ground (AUCg) estimates the magnitude of the cortisol response overall and area under the curve with respect to increase from baseline (AUCi) estimates the magnitude of the cortisol response from an individual's baseline. AUC calculations were completed using the following formulae (24) (m denoting single measurements, n denoting the total number of measurements):

$$AUC_G = \sum_{i=1}^{n-1} \frac{(m_{(i+1)} + m_i)}{2}$$

$$AUC_I = \left(\sum_{i=1}^{n-1} \frac{(m_{(i+1)} + m_i)}{2} \right) - (n-1) \cdot m_1$$

Independent component analysis of functional data

The set of five spatial maps (Fig. S1) from the group-average analysis were used to generate participant-specific versions of the spatial maps, and associated timeseries, using dual regression (25, 26). First, for each participant, the full set of independent component (IC) maps was regressed (as spatial regressors in a multivariate regression) into the participant's 4D task fMRI dataset. This resulted in a set of participant-specific timeseries, one per group IC spatial map. Next, those timeseries were regressed (as temporal regressors, again in a multiple regression) into the same 4D dataset, resulting in a set of participant-specific spatial maps, one per group-level spatial map. We then tested for within- and between-group differences using network modeling. First, we used the participant-specific timeseries from dual regression to create between-network connectivity matrices for each pair of networks using FSLNETS v0.6 (27) with non-aggressive removal of other network effects. To control for collinearity between the networks, we estimated partial correlation coefficients via Ridge Regression (with rho = 0.01) in FSLNets. Partial correlation r-values were converted to z-statistics with Fisher's transformation (28).

Network amplitude (how much a given network deviates from its own mean) was also estimated for each of the networks of interest, using the diagonal of the covariance matrix.

Supplemental Results

Affective Ratings

Group differences in affective response to stress were analyzed using mixed effects linear regression for state anxiety and visual analogue scales with a between-subjects factor of group (HC, MDD, rMDD) and within-subjects factor of time (pre and post stress) with a per-participant random adjustment to the fixed intercept (random intercept). For all affective rating measures there were significant main effects of stress and MDD group (Supplemental Table 3 and Fig S5), indicating that the stressor increased negative affect and decreased positive affect across participants, and that the MDD group had increased negative affect compared to the HC group. However, the group X stress interaction models only showed a trend or non-significant improvements in prediction (all model comparison *ps* < 0.07), suggesting the groups did not vary systematically in their affective responses to negative stress. As the difficulty of the MIST is set high to induce stress, accuracy in the MIST task typically reaches a floor and therefore is not analyzed.

Supplemental Discussion

We acknowledge stress induced by experimental procedures is possible, although participants carry out their MRS scan first and thus have been in the scanner for ~45 minutes before the onset of stress. This is at least two hours after IV insertion. Cortisol baselines are used from the beginning of the task, rather than out of the scanner to reduce any potential effect of stress from IV insertion or entering the scanner.

Supplemental Tables and Figures

	HC (N = 17)	MDD (N = 18)	rMDD (N = 14)	Significance (one-way ANOVA/ t-test)
Age (M, SD)	21.53 (2.45)	21.06 (1.76)	21.07 (2.12)	$p = 0.76$
Education years (M, SD)	15.06 (2.05)	15.00 (1.73)	14.86 (1.51)	$p = 0.95$
Annual Income (% under $50k)	41%	55%	50%	$p = 0.46$
Ethnicity (% Hispanic or Latinx)	12%	17%	29%	$p = 0.48$
Number of MDE's	0	2.84 (2.13)	1.53 (1.26)	$p = 0.05$[1]
BDI-II	0.71 (1.72)	27.20 (7.81)	1.21 (2.19)	$p < 0.001$
HDRS	0.59 (1.12)	17.3 (4.24)	1.00 (1.52)	$p < 0.001$
STAI-T	27.40 (6.38)	61.30 (8.84)	32.81 (9.22)	$p < 0.001$

Supplemental Table S1: Demographics

HC: Healthy Control; (r)MDD: (remitted) Major Depressive Disorder; BDI-II: Beck Depression Inventory(29); HDRS: Hamilton Depression Rating Scale(30); STAI-T: State-Trait Anxiety Inventory – Trait anxiety(4) (N is final sample analyzed) [1] P-value is based on a sample that includes one outlier in the MDD group (coded as 10 episodes) who described their number of episodes as "at least 10, too many to count".

Group	fMRI data	rACC GABA	DLPFC GABA	Cortisol	STAI	VAMS	PANAS
HC (N)	17	13	13	10	17	17	16
MDD (N)	18	17	17	14	16	18	15
rMDD (N)	14	13	13	10	13	13	13
Total	**49**	**43**	**43**	**34**	**46**	**48**	**44**

Supplemental Table S2: Final sample analyzed for each measure

fMRI: functional magnetic resonance imaging; rACC: rostral anterior cingulate cortex; DLPFC: dorsolateral prefrontal cortex; STAI-S: State-Trait Anxiety Inventory – State anxiety; VAMS: visual analogue measurement scale; PANAS: positive and negative affective schedule

Predictors	STAI-S β Estimates	STAI-S 95% CI	Negative PANAS β Estimates	Negative PANAS 95% CI	Positive PANAS β Estimates	Positive PANAS 95% CI	VAMS happy-sad β Estimates	VAMS happy-sad 95% CI	VAMS friendly-hostile β Estimates	VAMS friendly-hostile 95% CI	VAMS tense-relaxed β Estimates	VAMS tense-relaxed 95% CI
group [MDD]	19.504	[13.46, 25.56]	8.499	[5.25, 11.76]	-14.782	[-19.45, -10.1]	29.433	[17.00, 41.88]	16.495	[2.73, 30.25]	-23.258	[-35.61, -10.92]
group [rMDD]	2.303	[-4.27, 8.88]	0.75	[-2.72, 4.22]	-4.906	[-9.90, 0.09]	2.983	[-10.32, 16.29]	1.538	[-13.18, 16.25]	-2.934	[-16.17, 10.29]
stress [post-MAST]	8.638	[6.76, 10.50]	2.435	[1.00, 3.85]	-3.56	[-5.33, -1.76]	16.489	[12.09, 20.95]	15.909	[11.77, 20.06]	-25.311	[-31.79, -18.89]

Supplemental Table S3: Mixed effects regression analyses of self-report affective response to stress

Predictors	FPN β Estimates	FPN 95%CI	vmPFC-Strai-ACC β Estimates	vmPFC-Strai-ACC 95%CI	SN β Estimates	SN 95%CI
(Intercept)	0.8	[-0.03, 1.63]	0.74	[-0.07, 1.54]	0.72	[-0.33, 1.77]
group [MDD]	-0.2	[-0.40, -0.00]			0	[-0.26, 0.26]
group [rMDD]	-0.22	[-0.42, -0.01]			-0.14	[-0.40, 0.12]
time [post-Mast1]	0.03	[-0.13, 0.18]	-0.01	[-0.24, 0.21]	0.01	[-0.12, 0.15]
time [post-Mast2]	-0.15	[-0.30, 0.00]	0.21	[-0.02, 0.43]	0.05	[-0.09, 0.18]
time [post-Mast3]	-0.25	[-0.41, -0.10]	0.47	[0.24, 0.70]	0.02	[-0.12, 0.15]
rACC GABA	-0.04	[-0.57, 0.50]	0.54	[-0.14, 1.22]	0.35	[-0.42, 1.11]
DLPFC GABA	0.63	[-0.23, 1.48]			0.05	[-1.23, 1.32]
Cortisol AUCg	0.05	[-0.04, 0.14]			0.09	[-0.03, 0.20]
State anxiety change					0	[-0.02, 0.03]
Negative affect change					-0.02	[-0.05, 0.02]
Random Effects						
σ^2	0.09		0.28		0.06	
τ_{00}	0.01 subject		0.11 subject		0.03 subject	
ICC	0.11		0.28		0.28	
N	30 subject		43 subject		26 subject	
Observations	119		170		103	
Marginal R^2 / Conditional R^2	0.230 / 0.315		0.111 / 0.360		0.168 / 0.405	

Supplemental Table S4: Optimum models of network amplitude response to stress in MDD and rMDD, including rACC GABA, cortisol AUC and affective ratings as predictors
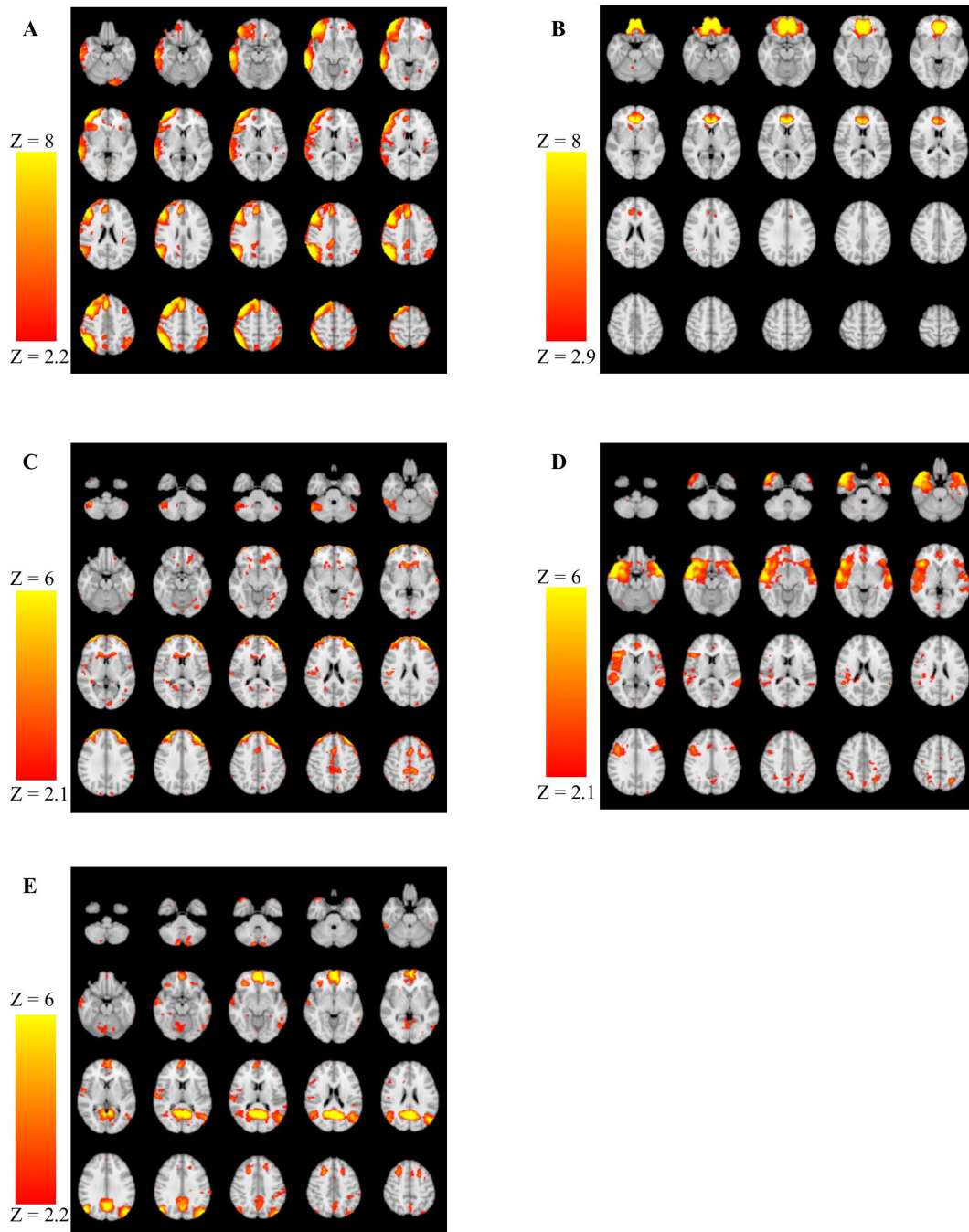
FPN: Right frontoparietal network; vmPFC-Str-ACC: Ventromedial prefrontal cortex, ventral striatum and anterior cingulate cortex; SN: Salience network (SN); DMN: Default mode network.
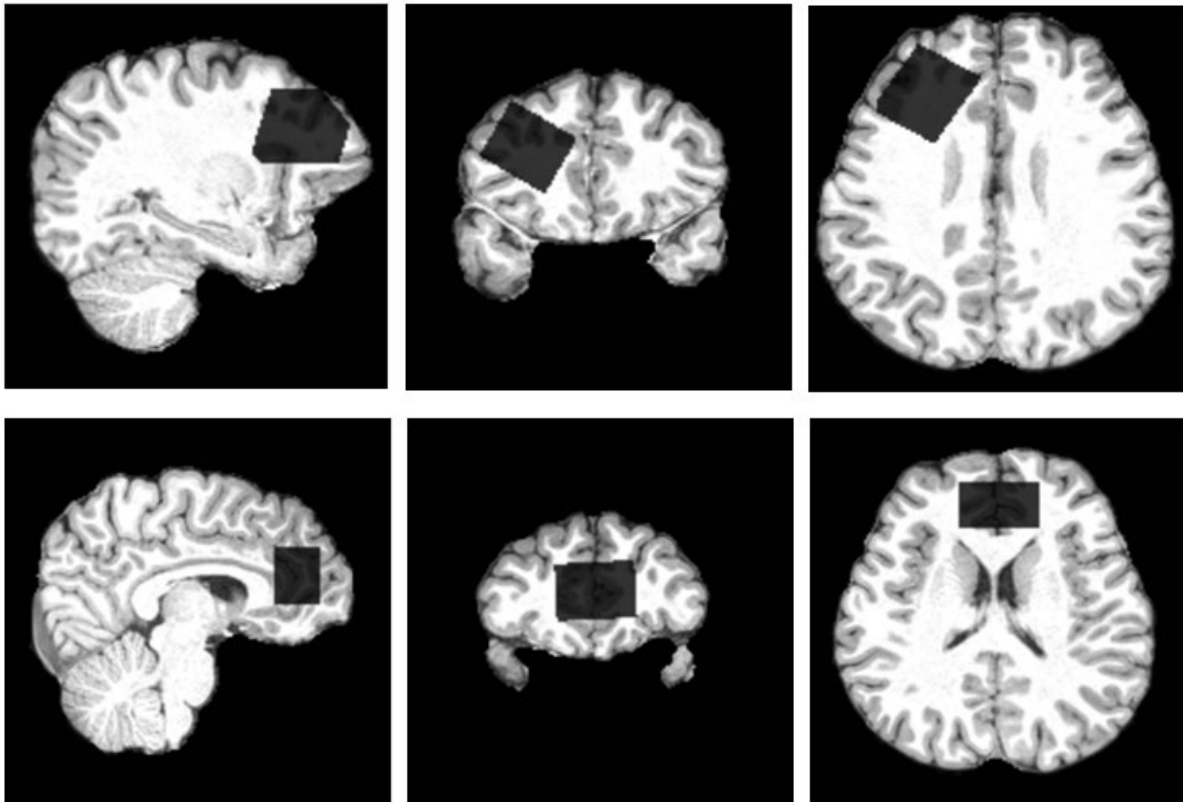
Supplemental Figure S1. Images illustrating the voxel placement for the (**A**) left dorsolateral prefrontal cortex (dlPFC) and (**B**) rostral anterior cingulate cortex (rACC). Voxel placement is presented in sagittal, coronal, and axial views on a single subject for each region.
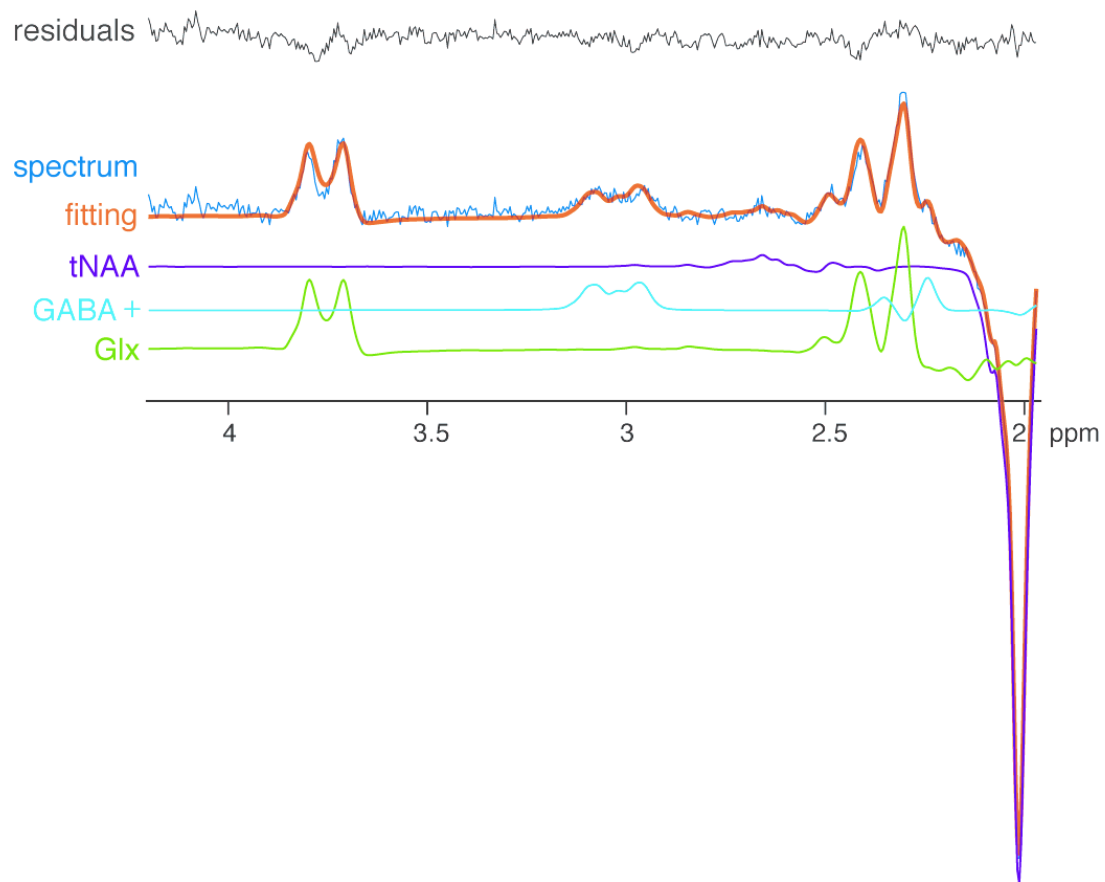
Supplemental Figure S2. GABA+-edited (difference) spectrum showing metabolite fitting lines as estimated with LCModel, depicting the GABA+-edited spectrum (dark blue), fitting line (orange), total NAA (tNAA; purple), GABA+ (light blue), glutamate+glutamine (Glx; green), and residuals (grey).

Supplemental Figure S3. Thresholded statistical maps of networks identified with group ICA. (A) Right frontoparietal network (FPN); (**B**) Ventromedial prefrontal cortex, ventral striatum and anterior cingulate cortex (vmPFC-Str-ACC); (**C**) Salience network (SN); (**D**) Temporal-insula-amygdala network (Temp-Ins-Amyg); (**E**) Default mode network (DMN).
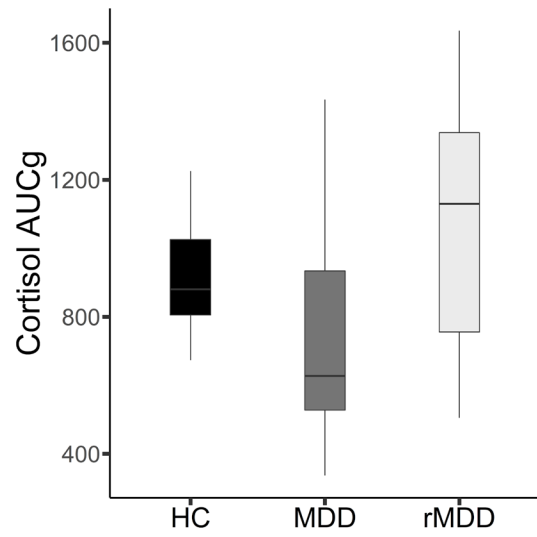
Supplemental Figure S4: Decreased cortisol AUCg in current versus remitted major depressive disorder

The dark line inside the box represents the median. The top of box is 75th percentile and bottom of box is 25th percentile. The end points of the lines (aka whiskers) are at a distance of 1.5 x Inter Quartile Range (the distance between 25th and 75th percentiles). HC (N = 10) mean (M) = 918, standard deviation (SD) = 168; MDD (N = 14) M = 737, SD = 319; rMDD (N = 10) M = 1076, SD = 371.
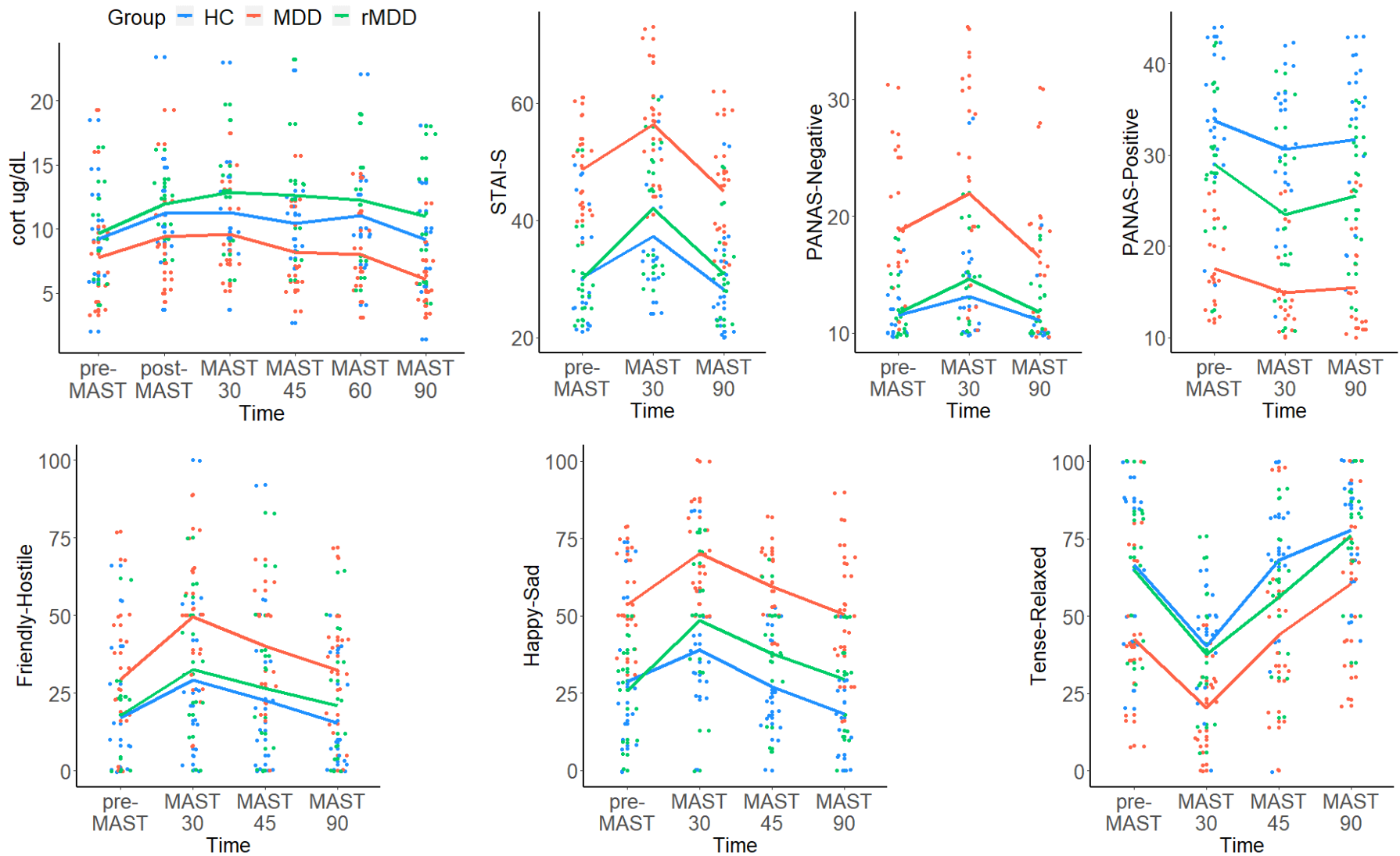
Supplemental Figure S5: Time course of cortisol and self-report affective rating changes from stress

STAI-S: State-Trait Anxiety Inventory (state); VAMS: Visual Analogue Measurement Scale; PANAS: Positive and Negative Affective Scale.

References:

1. Silveri MM, Cohen-Gilbert J, Crowley DJ, Rosso IM, Jensen JE, Sneider JT (2014): Altered anterior cingulate neurochemistry in emerging adult binge drinkers with a history of alcohol-induced blackouts. *Alcohol Clin Exp Res*. 38: 969–979.

2. Miller R, Stalder T, Jarczok M, Almeida DM, Badrick E, Bartels M, *et al.* (2016): The CIRCORT database: Reference ranges and seasonal changes in diurnal salivary cortisol derived from a meta-dataset comprised of 15 field studies. *Psychoneuroendocrinology*. 73: 16–23.

3. Watson D, Clark LA, Tellegen A (1988): Development and validation of brief measures of positive and negative affect: the PANAS scales. *J Pers Soc Psychol*. 54: 1063–1070.

4. Spielberger CD, Gorsuch RL, Lushene RE (1970): The State-Trait Anxiety Inventory. *MANUAL*. 1–23.

5. Tustison NJ, Avants BB, Cook PA, Zheng Y, Egan A, Yushkevich PA, Gee JC (2010): N4ITK: improved N3 bias correction. *IEEE Trans Med Imaging*. 29: 1310–1320.

6. Avants BB, Tustison N, Song G (2009): Advanced normalization tools (ANTS). *Insight j*. 2: 1–35.

7. Zhang Y, Brady M, Smith S (2001): Segmentation of brain MR images through a hidden Markov random field model and the expectation-maximization algorithm. *IEEE Trans Med Imaging*. 20: 45–57.

8. Dale AM, Fischl B, Sereno MI (1999): Cortical surface-based analysis: I. Segmentation and surface reconstruction. *Neuroimage*. 9: 179–194.

9. Klein A, Ghosh SS, Bao FS, Giard J, Häme Y, Stavsky E, *et al.* (2017): Mindboggling morphometry of human brains. *PLoS Comput Biol*. 13: e1005350.

10. Wang S, Peterson DJ, Gatenby JC, Li W, Grabowski TJ, Madhyastha TM (2017): Evaluation of field map and nonlinear registration methods for correction of susceptibility artifacts in diffusion MRI. *Front Neuroinform*. 11: 17.

11. Huntenburg JM (2014): Evaluating nonlinear coregistration of BOLD EPI and T1w images. .

12. Treiber JM, White NS, Steed TC, Bartsch H, Holland D, Farid N, *et al.* (2016): Characterization and correction of geometric distortions in 814 diffusion weighted images. *PLoS One*. 11: e0152472.

13. Greve DN, Fischl B (2009): Accurate and robust brain image alignment using boundary-based registration. *Neuroimage*. 48: 63–72.

14. Jenkinson M, Beckmann CF, Behrens TEJ, Woolrich MW, Smith SM (2012): FSL. *Neuroimage*. 62: 782–790.

15. Cox RW, Hyde JS (1997): Software tools for analysis and visualization of fMRI data. *NMR Biomed An Int J Devoted to Dev Appl Magn Reson Vivo*. 10: 171–178.

16. Lanczos C (1964): A precision approximation of the gamma function. *J Soc Ind Appl Math Ser B Numer Anal*. 1: 86–96.

17. Pruim RHR, Mennes M, van Rooij D, Llera A, Buitelaar JK, Beckmann CF (2015): ICA-AROMA: A robust ICA-based strategy for removing motion artifacts from fMRI data. *Neuroimage*. 112: 267–277.

18. Mescher M, Merkle H, Kirsch J, Garwood M, Gruetter R (1998): Simultaneous in vivo spectral editing and water suppression. *NMR Biomed*. 11: 266–272.

19. Mullins PG, McGonigle DJ, O'Gorman RL, Puts NAJ, Vidyasagar R, Evans CJ, *et al.* (2014): Current practice in the use of MEGA-PRESS spectroscopy for the detection of GABA. *Neuroimage*. 86: 43–52.

20. Tremblay S, Beaulé V, Proulx S, Lafleur LP, Doyon J, Marjańska M, Théoret H (2014): The use of magnetic resonance spectroscopy as a tool for the measurement of bi-hemispheric transcranial electric stimulation effects on primary motor cortex metabolism. *J Vis Exp*. 93.

21. Marjańska M, Lehéricy S, Valabrègue R, Popa T, Worbe Y, Russo M, *et al.* (2013): Brain dynamic neurochemical changes in dystonic patients: A magnetic resonance spectroscopy study. *Mov Disord*. 28: 201–209.

22. Duda JM, Moser AD, Zuo CS, Du F, Chen X, Perlo S, *et al.* (2021): Repeatability and reliability of GABA measurements with magnetic resonance spectroscopy in healthy young adults. *Magn Reson Med*. 85: 2359–2369.

23. Pruessner JC, Dedovic K, Khalili-Mahani N, Engert V, Pruessner M, Buss C, *et al.* (2008): Deactivation of the limbic system during acute psychosocial stress: evidence from positron emission tomography and functional magnetic resonance imaging studies. *Biol Psychiatry*. 63: 234–240.

24. Pruessner JC, Kirschbaum C, Meinlschmid G, Hellhammer DH (2003): Two formulas for computation of the area under the curve represent measures of total hormone concentration versus time-dependent change. *Psychoneuroendocrinology*. 28: 916–931.

25. Beckmann CF, Mackay CE, Filippini N, Smith SM (2009): Group comparison of resting-state FMRI data using multi-subject ICA and dual regression. *Neuroimage*. 47: S148.

26. Filippini N, MacIntosh BJ, Hough MG, Goodwin GM, Frisoni GB, Smith SM, *et al.* (2009): Distinct patterns of brain activity in young carriers of the APOE-ε4 allele. *Proc Natl Acad Sci*. 106: 7209–

7214.

27. Smith SM, Vidaurre D, Beckmann CF, Glasser MF, Jenkinson M, Miller KL, *et al.* (2013): Functional connectomics from resting-state fMRI. *Trends Cogn Sci*. 17: 666–682.

28. Smith SM, Miller KL, Salimi-Khorshidi G, Webster M, Beckmann CF, Nichols TE, *et al.* (2011): Network modelling methods for FMRI. *Neuroimage*. 54: 875–891.

29. Beck AT, Steer RA, Brown GK (1996): Beck Depression Inventory-II (BDI-II). *San Antonio, TX Psychol Corp.* .

30. Montgomery SA, Asberg M (1979): A new depression scale designed to be sensitive to change. *Br J Psychiatry*. 134: 382–389.